SOI: 1.1/TAS DOI: 10.15863/TAS
International Scientific Journal
Theoretical & Applied Science

p-ISSN: 2308-4944 (print) **e-ISSN:** 2409-0085 (online)

Year: 2026 **Issue:** 02 **Volume:** 154

Received: 26.02.2026
Accepted/Published: 28.02.2026
https://T-Science.org

Issue Article

Denis Chemezov
Vladimir Polytechnic College
MEng, Honorary Worker of the Education Field of the Russian Federation, Academician of International Academy of Theoretical and Applied Sciences, Lecturer, Russian Federation
https://orcid.org/0000-0002-2747-552X
vpk-science@yandex.ru

Anzhelika Bayakina
Vladimir Polytechnic College
Lecturer, Russian Federation

Darya Mishakova
Vladimir Polytechnic College
Student, Russian Federation

Artyom Armyakov
Vladimir Polytechnic College
Student, Russian Federation

Ilyas Evstigneev
Vladimir Polytechnic College
Student, Russian Federation

Sergey Bezrukov
Vladimir Polytechnic College
Student, Russian Federation

Danil Simachkov
Vladimir Polytechnic College
Student, Russian Federation

Danil Isaev
Vladimir Polytechnic College
Student, Russian Federation

Vladislav Markin
Vladimir Polytechnic College
Student, Russian Federation

FORECAST OF STRAIN INTENSITY OF A THIN-WALLED STEEL BUSHING AT A PRESSING LENGTH OF UP TO 100 MM WITH GUARANTEED INTERFERENCE

Impact Factor: ISRA (India) = 6.317 | ISI (Dubai, UAE) = 1.582 | GIF (Australia) = 0.564 | JIF = 1.500 | SIS (USA) = 0.912 | РИНЦ (Russia) = 0.191 | ESJI (KZ) = 8.100 | SJIF (Morocco) = 6.004 | ICV (Poland) = 6.630 | PIF (India) = 1.940 | IBI (India) = 4.260 | OAJI (USA) = 0.350

Abstract: *Using the Comsol Multiphysics software package, the dynamics of pressing a steel shaft into a steel bushing was simulated, ensuring a fit with a guaranteed interference of 0.1 mm. For a thin-walled bushing, a prediction of the intensity of stresses and strains in the material was made.*

Key words: *guaranteed interference, pressing length, bushing model, shaft model, strain, pressure, contact force.*

Language: *English*

Citation: Chemezov, D., et al. (2026). Forecast of strain intensity of a thin-walled steel bushing at a pressing length of up to 100 mm with guaranteed interference. *ISJ Theoretical & Applied Science, 02 (154),* 75-84.

Soi: https://s-o-i.org/1.1/TAS-02-154-12 ***Doi***: crossref https://dx.doi.org/10.15863/TAS.2026.02.154.12

Scopus ASCC: *2206.*

1. Introduction

An interference fit is a method of assembling two parts, usually a shaft and a hole, in which the inside diameter of the hole is slightly smaller than the outside diameter of the shaft. During assembly, the parts fit tightly together due to friction and deformation, which ensures a reliable and durable connection without the use of additional fasteners. This method is widely used in mechanical engineering, such as in the manufacture of gears, bearings and pulleys, to ensure stability and precise alignment.

Pressing-in of parts with guaranteed interference can cause a number of problems, including difficulty in assembly and disassembly due to high friction, the possibility of component damage such as warping or cracking during installation, misalignment resulting in uneven load distribution, and dimensional changes caused by thermal expansion or contraction that can lead to poor fit.

When pressing-in of parts with guaranteed interference, the bushing material is subjected to triaxial loading. Radial stress results in a compressive stress acting perpendicular to the joint surface. Tangential stress acts along the arc of a circle and leads to dangerous stretching of the bushing material (the appearance of cracks on the end of the part, cracking of the material along the axis of the part). The axial load causes shear and stretching of the bushing material.

A priori analysis of studies on the manufacture of parts to ensure guaranteed interference and their assembly allowed us to identify a number of problematic issues and ways to solve them. In the article [1], the author presents a comprehensive concept for designing interference fits that include elastic-plastic components. The paper presents a general formulation for the analysis of stress and strain behavior in such joints, taking into account the complex interaction between elastic and plastic deformation. The article by Teng, Zhang, Zhou and Xu [2] deals with the mechanical properties and design methods of cylindrical interference fits. It examines the stress and strain characteristics associated with such fits, presents analytical models for predicting these properties, and offers design recommendations for optimizing interference fit performance in engineering applications. Zhang, McClain, and Fang [3] discuss the design of interference fits using the finite element method. The stresses and strains used in the design of optimal interference fits for mechanical components are analyzed and a detailed numerical approach is proposed to predict the behavior of such fits under various loading conditions. An experimental study of the connection of mechanical components with interference, aimed at understanding the behavior and performance characteristics of such connections under various conditions, is presented in [4]. The authors investigate factors affecting the strength and reliability of interference joints, including contact pressures and deformation characteristics, through a series of laboratory experiments. In the article by Mustafin et al. [5], a comparative analysis of the quality of fitting of parts with guaranteed interference on shafts is carried out, in which the main attention is paid to both annular and solid sections. The study [6] combined experimental and analytical approaches to evaluate the influence of roughness characteristics on load transfer and interference fit stability in mechanical assemblies. Papers [7-8] investigate how surface roughness affects contact mechanics, which provides insight into stress distribution and contact behavior under different conditions. In [9], a theoretical analysis with experimental verification was performed to develop a prediction tool that improves the understanding of pressing-in characteristics, which ultimately contributes to more efficient and safer assembly of railway components. In a paper published by You et al. [10], the pressing-in quality in the pressing-in assembly process was predicted by analyzing the pressing curve and the maximum pressing force. In their study [11], the authors focus on the mechanisms of fretting fatigue, analyze the influence of various parameters such as load, contact pressure and material properties, and provide experimental and theoretical data on increasing the service life of interference fits. A new analytical approach to predicting the pressing curve of components with interference fit is presented in [12]. The proposed method extends the capabilities of existing models by providing more accurate predictions of interference fit characteristics, providing valuable information for materials processing and production optimization.

The purpose of this article was to evaluate the deformed state of a steel bushing under conditions of pressing-in a steel shaft into it while ensuring guaranteed interference. Modeling the dynamics of the technological process will allow us to determine the critical conditions for performing an assembly based on the pressing length criterion.

2. Materials and methods

To quantitatively evaluate the stress and strain state of the material of a thin-walled bushing under pressing-in conditions, an experiment was carried out using the finite element modeling method in the Comsol Multiphysics software package. The simulation conditions included the creation of two-dimensional models of the shaft and the bushing of equal length of 100 mm on the *XY* plane. The difference in seating dimensions (diameters) is accepted as 0.1 mm, which indicates a guaranteed interference. The wall thickness of the bushing model was taken to be 10 mm, in order to obtain a thin-walled product. Precise centering of the paired models was ensured by creating chamfers measuring 1×45° along the edges of the end parts of the shaft and bushing. The values of the force for pressing-in of the shaft model into the bushing model were calculated every 5 mm of the pressing length and are presented in Section 3 of this article. The action of the pressing force was directed along the *Y* coordinate axis. The pressing length was taken as 100 mm. The pressing-in of part models was carried out without preliminary heating. The conditions for simulating the pressing-in process are shown in the Figure 1.

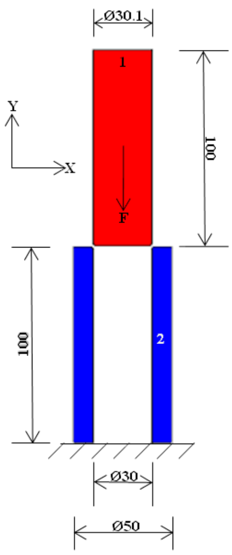

Figure 1. Conditions for simulating the pressing-in process of the shaft model into the bushing model with guaranteed interference. The diagram shows the following symbols: *1* – shaft model in longitudinal section, *2* – bushing model in longitudinal section, *F* – pressing force.

The shaft and bushing models were given the properties of 1040 steel at 20°C: density – 7845 kg/m³, tensile strength – 600 MPa, yield strength – 500 MPa, elongation – 12%, hardness (HB) – 195, Young's modulus – 200 GPa, Poisson's ratio – 0.29.

Both models have the properties of an isotropic material. The mathematical formulation of the isotropic material model is represented by the following equations (1-8):

$$0 = \nabla \cdot (FS)^T + F_V \ (1)$$
$$F = I + \nabla u \ (2)$$
$$S = S_{ad} + C : \epsilon_{el} \ (3)$$
$$\epsilon_{el} = \epsilon - \epsilon_{inel} \ (4)$$
$$\epsilon_{inel} = \epsilon_0 + \epsilon_{ext} + \epsilon_{th} + \epsilon_{hs} + \epsilon_{pl} + \epsilon_{cr} + \epsilon_{vp} + \epsilon_{ve} \ (5)$$
$$S_{ad} = S_0 + S_{ext} + S_q \ (6)$$
$$\epsilon = \frac{1}{2}[(\nabla u)^T + \nabla u + (\nabla u)^T \nabla u] \ (7)$$
$$C = C(E, \nu) \ (8)$$

where ∇ is gradient, *F* is deformation gradient tensor, *S* is the second Piola-Kirchhoff stress, *T* is the transpose of the tensor, F_V is body force, *I* is the unit tensor, *u* is displacement vector, S_{ad} is total (additive) stress, *C* is the 4th order elasticity tensor, *:* is double dot product; ϵ_{el} is elastic strain, ϵ is total strain, ϵ_{inel} is inelastic strain, ϵ_0 is initial strain, ϵ_{ext} is external strain, ϵ_{th} is thermal strain, ϵ_{hs} is hygroscopic swelling, ϵ_{pl} is plastic strain, ϵ_{cr} is creep strain, ϵ_{vp} is viscoplastic strain, ϵ_{ve} is viscoelastic strain, S_0 is initial stress, S_{ext} is external stress, S_q is extra stress, *E* is Young's modulus, υ is Poisson's ratio.

The formulation of the initial values for the displacement and velocity fields is presented by equations (9-11):

$$u_0 = -r(1 - cos\phi) + (e_z \times r)sin\phi + u \ (9)$$
$$\left(\frac{\partial u}{\partial t}\right)_0 = \left(e_z \times (r + u_0 - u)\right)\frac{\partial \phi}{\partial t} + \frac{\partial u}{\partial t} \ (10)$$
$$r = (X - X_c) \ (11)$$

where u_0 is initial displacement field, $-r(1 - cos\varphi)$ is radial component of displacement, $(e_z \times r)sin\varphi$ is tangential component of displacement, *t* is time, *X* is current coordinates (material or spatial), X_c is coordinates of the center of rotation.

The bushing model was based on a flat surface at the end. Thus, the constraint for fixing the bushing model can be represented as $u = 0$.

The contact surfaces were the outer diameter of the shaft model and the diameter of the hole of the bushing model. The contact surfaces of models may penetrate each other slightly depending on a certain contact rigidity, which links the penetration with the resulting reactive forces. Mathematically, this can be written by the following equations (12-14):

$$T_n = if(g_n \leq 0, -p_n, g_n, 0) + if(g_{n,old} \leq 0, -p_{nv} \min\left(\frac{\partial g_n}{\partial t}, 0\right), 0) \quad (12)$$

$$p_n = f_p \frac{E_{char}}{h_{min}} \quad (13)$$

$$p_{nv} = \tau_n \frac{E_{char}}{h_{min}} \quad (14)$$

where T_n is contact pressure, g_n is the shortest distance between the points of the “nested” (slave/destination) and “main” (master/source) surfaces along the normal vector, p_n is contact pressure penalty factor, $g_{n,old}$ is gap value at the previous iteration step, p_{nv} is viscous contact pressure penalty factor, f_p is penalty factor multiplier, E_{char} is characteristic Young's modulus, h_{min} is minimum element size, τ_n is damping time scale.

The calculation was performed taking into account the specified models of wear, friction and slip velocity.

The wear model of the contact surfaces of the shaft and bushing is represented by the following formulations of the deformed geometry: wear model – generalized Archard, wear constant – 0.0001, exponent – 1, wear surface – destination.

The friction parameters between the contact surfaces of the shaft and bushing models included: friction model – Coulomb, friction coefficient – 0.5, cohesion sliding resistance – 0, maximum tangential traction – default value (infinity). The friction of the contact surfaces of models is simulated using the following formulas (15-18):

$$T_{t,trial} = T_{t,old} - p_t \frac{\partial g_t}{\partial t} \quad (15)$$

$$T_t = \min\left(\frac{T_{t,crit}}{|T_{t,trial}|}, 1\right) T_{t,trial} \quad (16)$$

$$T_{t,crit} = \min(\mu T_n + T_{cohe}, T_{t,max}) \quad (17)$$

$$p_t = f_t \frac{E_{char}}{3h_{min}} \quad (18)$$

where $T_{t,trial}$ is trial tangential stress, $T_{t,old}$ is value of tangential stress from the previous converged step (in non-stationary problems) or the previous iteration, p_t is friction force penalty factor, g_t is tangential slip, T_t is friction force, $T_{t,crit}$ is tangential friction force during sliding, μ is friction coefficient, T_{cohe} is cohesion sliding resistance, $T_{t,max}$ is maximum tangential traction, f_t is penalty factor multiplier.

The slip velocity of the contact surfaces of models is represented by equation (19):

$$T_t = \min(\mu T_n + T_{cohe}, T_{t,max}) \frac{-v_{slip}}{|v_{slip}|} \quad (19)$$

where v_{slip} is slip velocity.

The quality and accuracy of the simulation results were high due to the generation of a mesh on the shaft and bushing models with the following statistics: minimum element quality – 0.7567, average element quality – 0.9849, triangle – 3204, edge element – 354, vertex element – 16, maximum element size – 2.01, minimum element size – 0.00402, curvature factor – 0.2.

3. Results and discussion

The results of finite element modeling of the pressing-in process of the shaft into the bushing while ensuring guaranteed interference are presented in the Table 1.

Table 1. Results of finite element modeling of the process: the first column is the pressing length of the shaft model into the bushing model, the second column is the distribution of equivalent deviatoric strain of the bushing material during pressing-in, and the third column is the distribution of pressure in the bushing material during pressing-in.

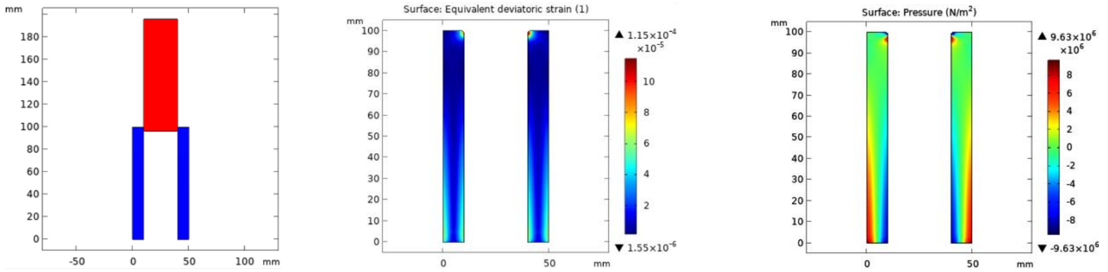

Pressing length is 5 mm

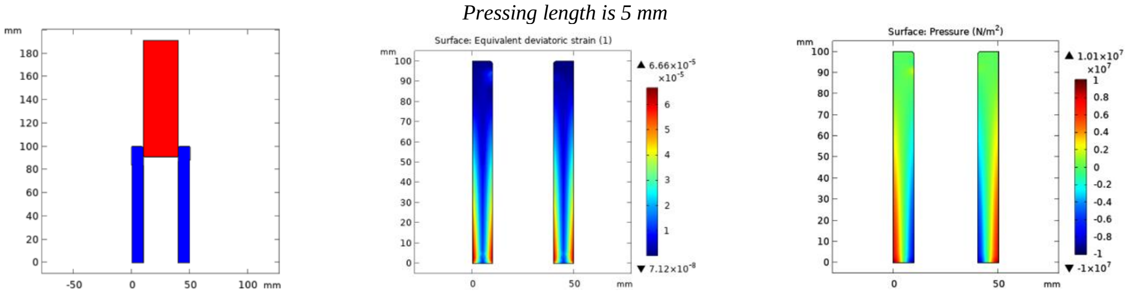

Pressing length is 10 mm

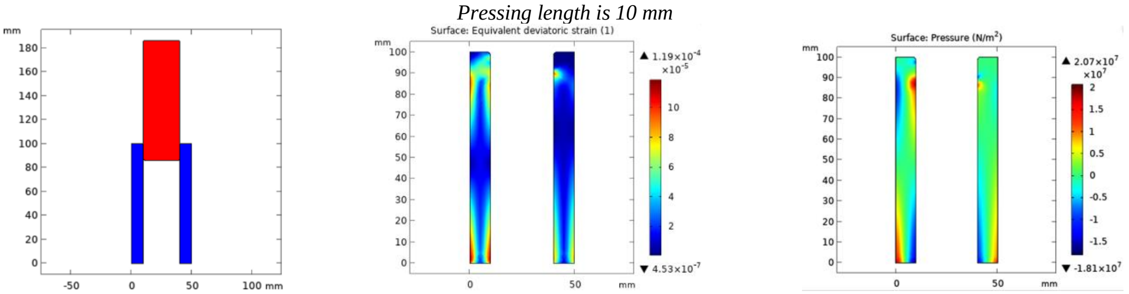

Pressing length is 15 mm

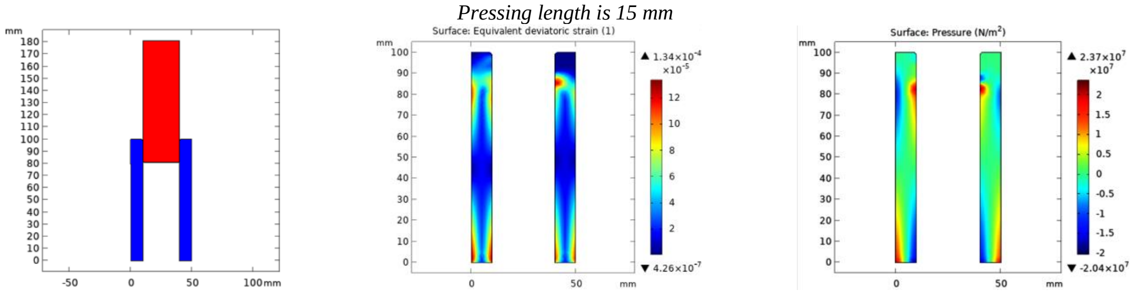

Pressing length is 20 mm

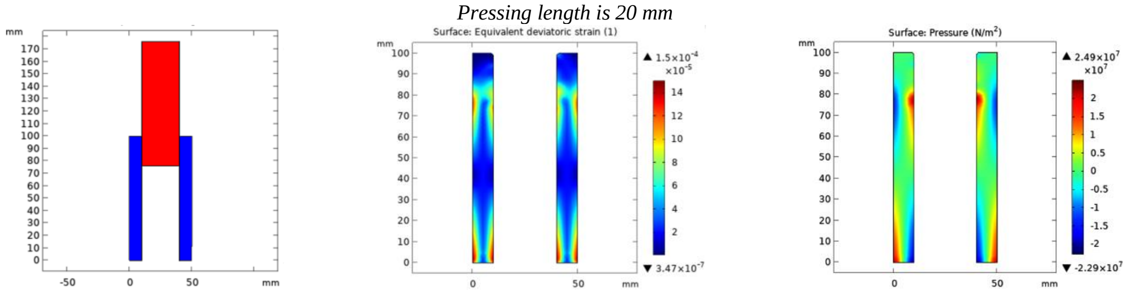

Pressing length is 25 mm

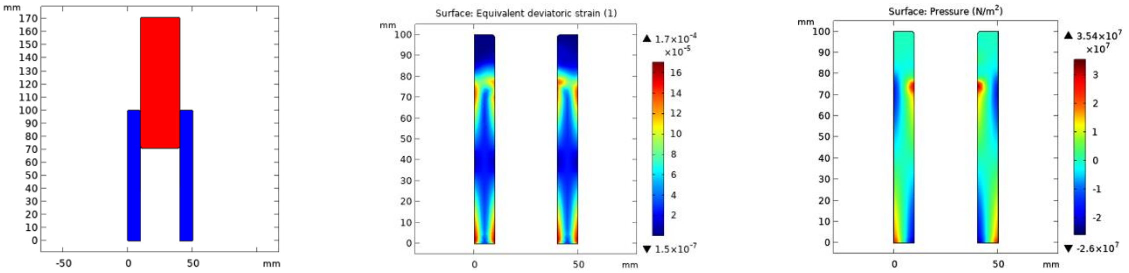

Pressing length is 30 mm

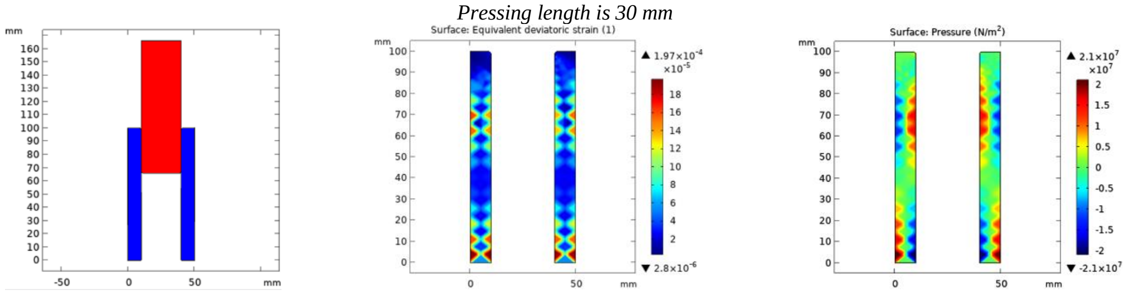

Pressing length is 35 mm

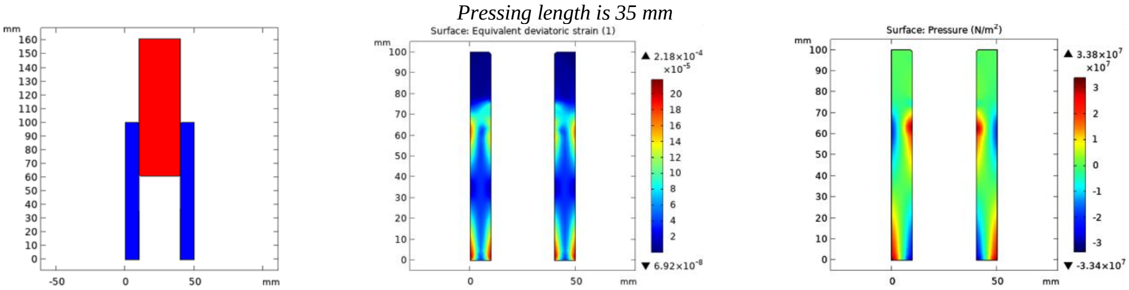

Pressing length is 40 mm

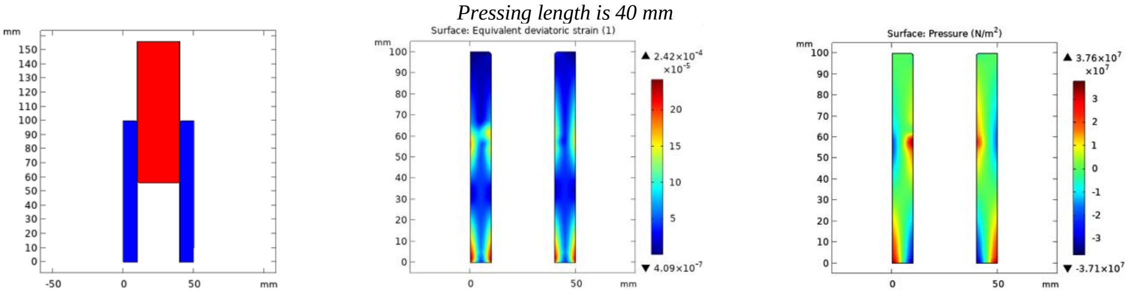

Pressing length is 45 mm

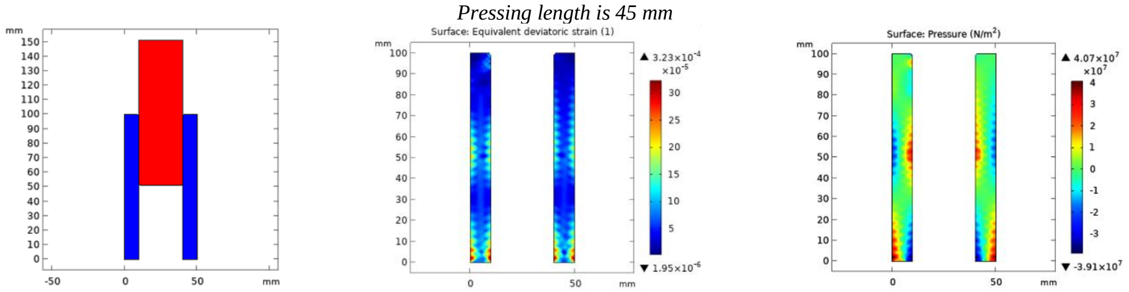

Pressing length is 50 mm

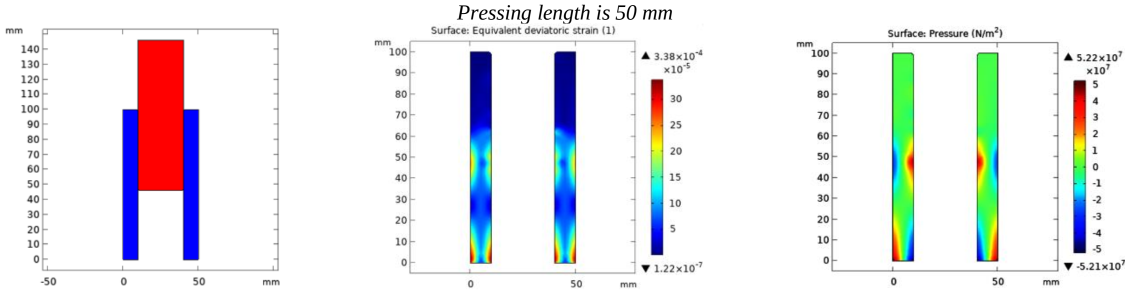

Pressing length is 55 mm

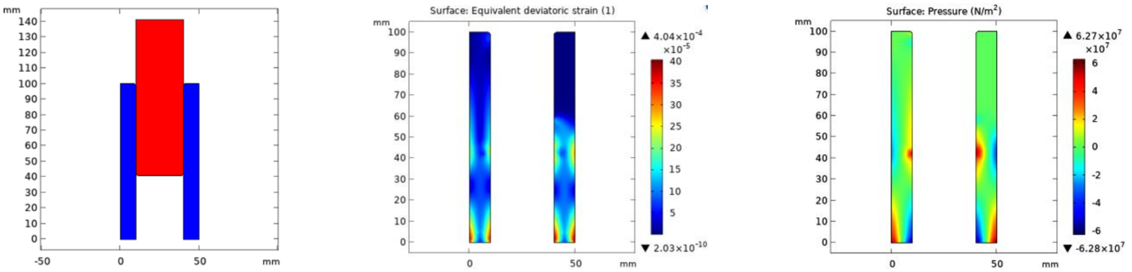

Pressing length is 60 mm

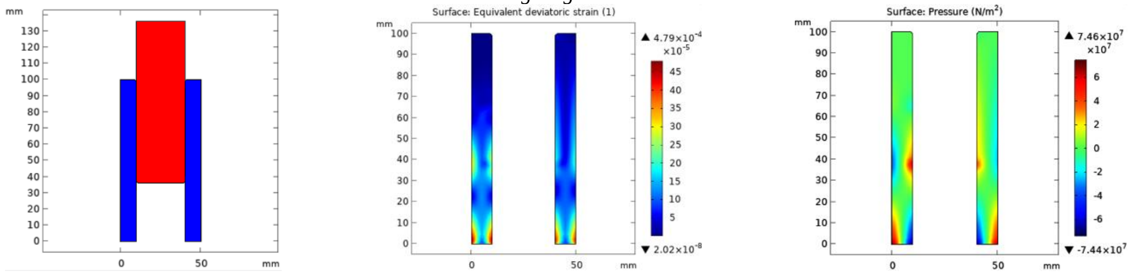

Pressing length is 65 mm

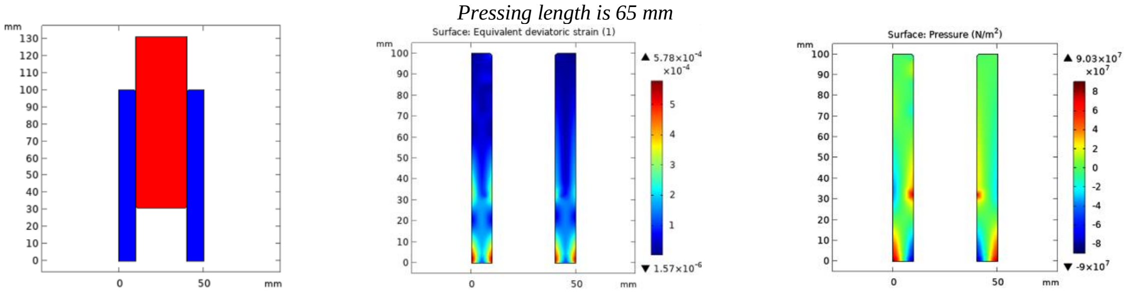

Pressing length is 70 mm

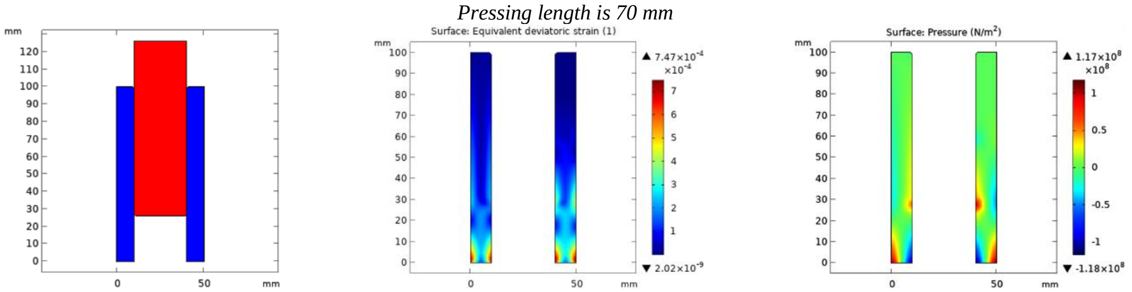

Pressing length is 75 mm

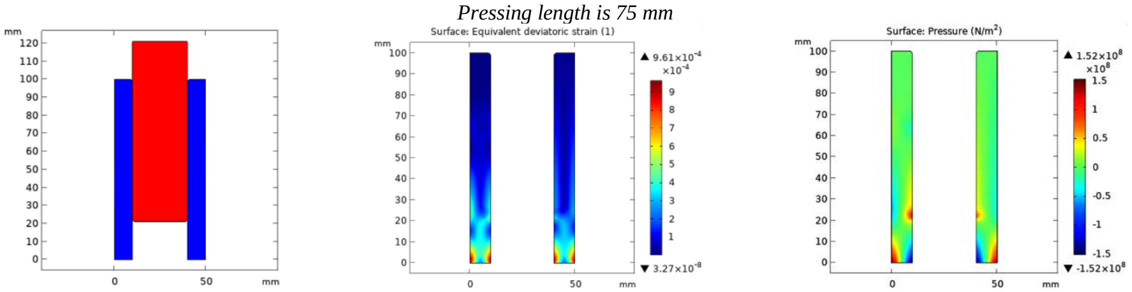

Pressing length is 80 mm

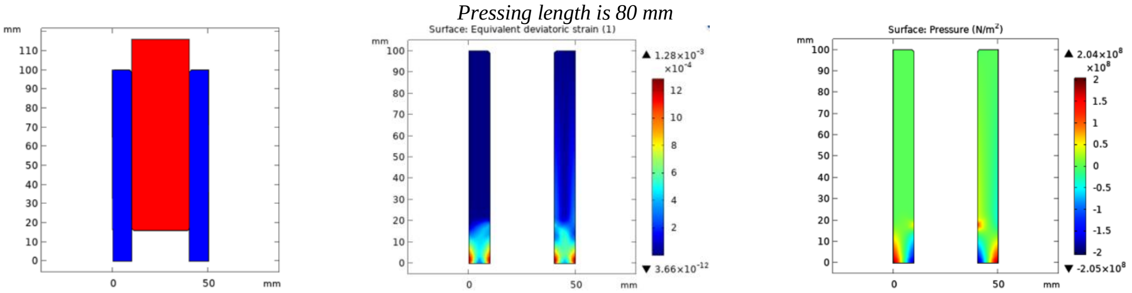

Pressing length is 85 mm

Impact Factor:

ISRA (India)	= **6.317**	**SIS** (USA)	= **0.912**	**ICV** (Poland)	= **6.630**
ISI (Dubai, UAE)	= **1.582**	**РИНЦ** (Russia)	= **0.191**	**PIF** (India)	= **1.940**
GIF (Australia)	= **0.564**	**ESJI** (KZ)	= **8.100**	**IBI** (India)	= **4.260**
JIF	= **1.500**	**SJIF** (Morocco)	= **6.004**	**OAJI** (USA)	= **0.350**

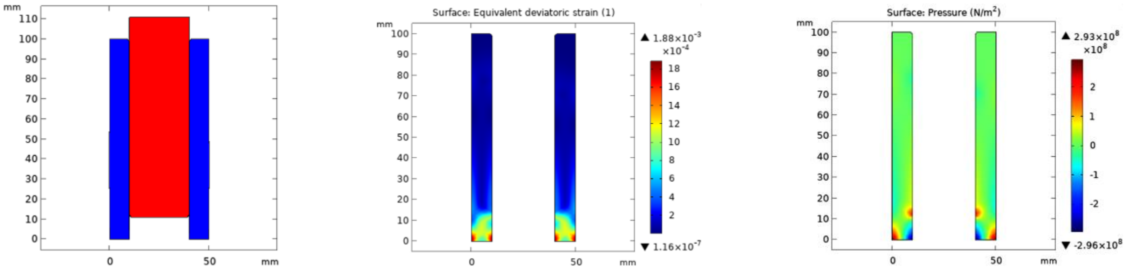

Pressing length is 90 mm

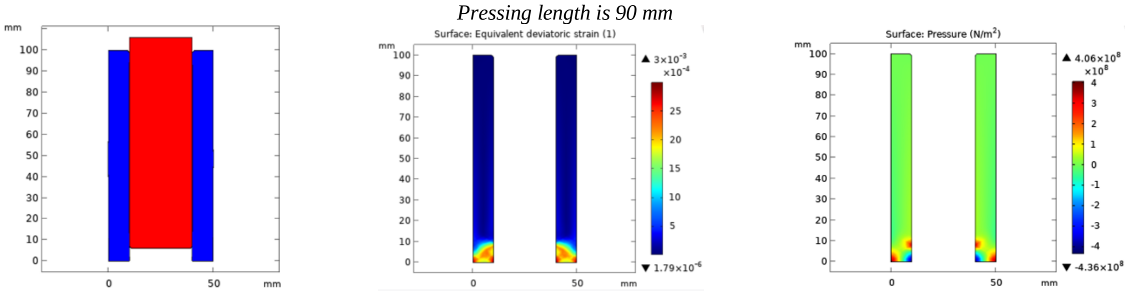

Pressing length is 95 mm

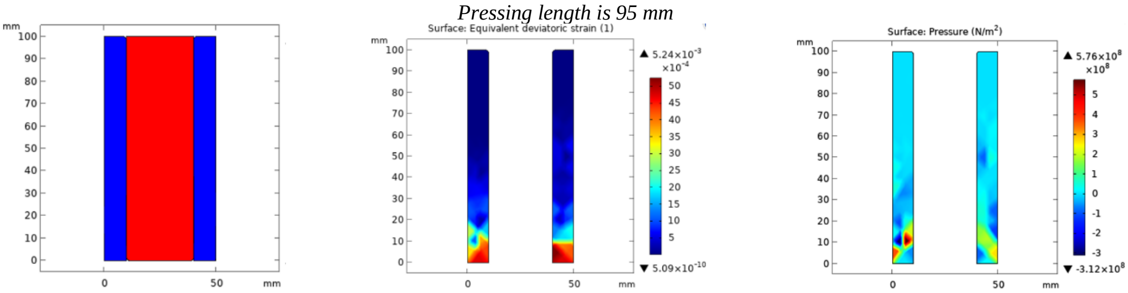

Pressing length is 101 mm

The table shows the diagrams of sequential pressing-in of part models over the entire length with a step of 5 mm, the distribution of equivalent deviatoric strain and pressure of the material of the bushing model during pressing-in.

Equivalent deviatoric strain characterizes the change in the shape of the bushing model without changing its volume. The intensity of the change in shape is expressed by a coefficient. As the shaft model is pressed into the bushing model, strains of greater intensity are noted in the latter in the contact zone and on the outer surface of the bushing model, as well as on the inner and outer surfaces of the lower part of the bushing model. A sharp increase in the peak values of equivalent deviatoric strain over a pressing length of 10 to 40 mm was determined at a depth of 2 to 5 mm from the wall thickness of the bushing model. A more uniform distribution of strain is observed in subsequent steps of the pressing-in process and reaches its maximum value at a pressing length of 101 mm across the entire thickness of the bushing model in the contact zone.

The pressure distributions in the material of the bushing model are obtained in positive and negative values, which correspond to compression and tension, respectively. The tension and compression of the bushing model material are almost identical in absolute value, with the exception of the pressing-in steps of 30 mm and 101 mm. This is due to the greatest deformation of the shape of the bushing model at the specified steps. As the shaft model is pressed into place, compression occurs on the inner contact surface of the bushing model. In this case, on the outer surface of the bushing model, the pressure changes from tension to compression over a pressing length of 85 mm. Complete pressing-in of the shaft model into the bushing model is characterized by almost complete compression of the bushing model material by 5.76×10^{8} N/m^{2}.

Figure 2 shows the dependencies of the total contact force on the pressing length along the *X* and *Y* coordinate axes.

Positive and negative values of contact force on the graphs characterize the compressive force and tensile force along the corresponding coordinate axes, respectively. Radial stresses arise along the *X* coordinate axis, causing the material of the bushing and shaft models to be compressed, while axial stresses arise along the *Y* coordinate axis, causing shear and stretching of the material of the bushing model.

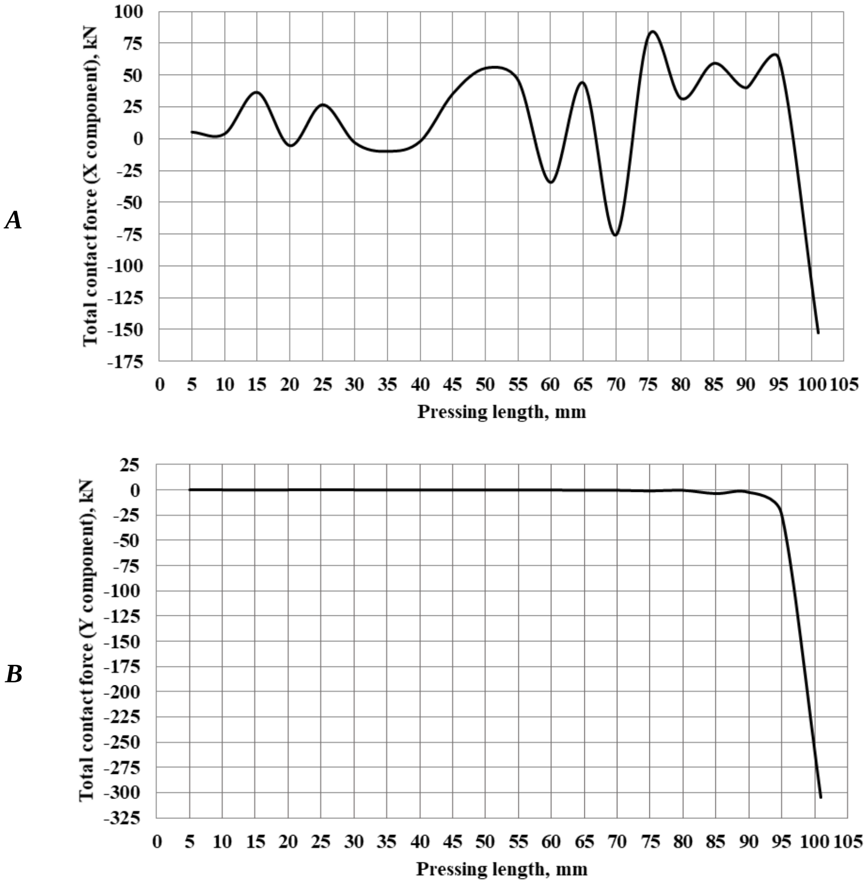

Figure 2. Dependencies of the total contact force along the pressing length: *A* – along the *X* coordinate axis, *B* – along the *Y* coordinate axis.

The radial force is variable in sign over the calculated pressing length, which indicates a complex stress state of the bushing model. At a pressing length of the shaft model into the bushing model of up to 45 mm, a relatively stable compressive stress of the material is observed. Further pressing-in of the shaft model into the bushing model is caused by sharp changes in the contact force with a critical value of up to -152.66 kN over a pressing length of 101 mm.

The axial contact force is always negative (tensile) and varies in the range from 4.3×10^{-5} to -1.05 kN over a pressing length of up to 75 mm. The contact force increases sharply to a maximum value of -304.53 kN over a pressing length of 75 to 101 mm, which may lead to the risk of cracking in the axial direction.

4. Conclusion

Based on the analysis of the results of computer simulation of the pressing-in process of the shaft model into the bushing model while ensuring guaranteed interference, the following conclusions can be drawn:

1. Pressing-in of parts without preheating ensures minimal changes in the geometry of the bushing, with the compression of the material predominantly in the radial and axial directions.
2. The pressing length (up to 45 mm) at which the process of joining parts is stable has been determined. At a pressing length of 45 to 70 mm, sharp changes in the value of the contact force occur, which arise due to an increase in the contact area of surfaces being joined. The pressing-in process becomes unstable due to the occurrence of plastic deformations and a significant increase in the friction force on the contact surfaces. The risk of partial failure of the bushing is determined in the range of a pressing length of 75-101 mm. The most dangerous stress state of the material is determined in the axial direction at the end of the pressing length range, leading to catastrophic tension of the bushing.

The recommended conditions for pressing-in of the shaft into the bushing ensure a reliable, permanent connection of the mechanism parts, guaranteeing its trouble-free operation under heavy loads, including dynamic ones.

References:

1. Baldanzini, N. (2004). A general formulation for designing interference-fit joints with elastic-plastic components. *J. Mech. Des., 126*, 737-743.
2. Teng, R. J., Zhang, Y. B., Zhou, X. J., & Xu, Z. N. (2012). Mechanical properties and design method of cylindrical interference fit. *Chin. J. Mech. Eng., 48*, 160-166.
3. Zhang, Y., McClain, B., & Fang, X. D. (2000). Design of interference fits via finite element method. *International Journal of Mechanical Sciences, Vol. 42, Issue 9*, 1835-1850.
4. Mikolainis, J., & Bakšys, B. (2012). Experimental investigation of interference fit connection of mechanical components. *Journal of Vibroengineering, Vol. 14, No. 1*, 73-78.
5. Mustafin, A., Sadykov, N., Kabylkaiyr, D., Shaimardan, A., & Sadykova, A. (2024). Comparative Analysis of Fits of Parts with Guaranteed Interference on Shafts of Annular and Solid Sections. *Material and Mechanical Engineering Technology, №3*, 112-116.
6. Sogalad, L., & Udupa, N. G. S. (2009). Load bearing ability of interference-fitted assemblies: a roughness profile analysis. *Proc. Inst. Mech. Eng. Part C-J. Eng. Mech. Eng. Sci., 223*, 1623-1633.
7. Yang, G. M., Coquille, J. C., Fontaine, J. F., & Lambertin, M. (2002). Contact pressure between two rough sourfaces of cylindrical fit. *J. Mater. Process. Technol., 3(5)*, 490-497.
8. Yang, G. M., Coquille, J. C., Fontaine, J. F., & Lambertin, M. (2001). Influence of roughness on characteristics of tight interference fit of a shaft and a hub. *International Journal of Solids and Structures, Volume 38, Issues 42-43*, 7691-7701.
9. Benuzzi, D., & Donzella, G. (2004). Prediction of the press-fit curve in the assembly of a railway axle and wheel. *Proc. Inst. Mech. Eng. Part F-J. Rail Rapid Transit, 218*, 51-65.
10. You, B., Lou, Z. F., Luo, Y., Xu, Y., & Wang, X. D. (2015). Prediction of pressing quality for press-fit assembly based on press-fit curve and maximum press-mounting force. *Int. J. Aerosp. Eng.*, Article ID 823019823019.
11. Huang, C. W., Yang, G. X., Fu, N. J., & Xie, J. L. (2013). Research on fretting fatigue life of interference fit and its influencing factors. *In: International Conference on Mechatronics and Materials Engineering*, 293-300.
12. Wang, X. Y., Lou, Z. F., Wang, X. D., & Xu, C. L. (2017). A new analytical method for press-fit curve prediction of interference fitting parts. *J. Mater. Process. Technol., 250*, 16-24.